Total variation regularization with Split Bregman based method in magnetic induction tomography using experimental data

F Li[1], JFPJ Abascal[2,3], M Desco[2,3,4], M Soleimani[1]

Abstract-Magnetic induction tomography (MIT) is an imaging modality with a wide range of potential applications due to its non-contact nature. MIT is a member of the electrical tomography family that faces the most difficult imaging challenges, due to its demanding measurement accuracy requirements and its difficult forward and inverse problems. This paper presents for the first time split Bregman total variation (TV) regularization to solve the MIT inverse problem. Comparative evaluations are presented between proposed TV algorithm and more commonly used Tikhonov regularization method. Tikhonov regularization which is based on the $l_2 - norm$ is solved linearly while TV is solved using the Split Bregman formulation, which has been shown to be optimal for $l_1 - norm$ regularization. Experimental results are quantified by a number of image quality measurements, which show the superiority of the proposed TV method both on low conductivity and high conductivity MIT data. Significant improvement in MIT imaging results will make the proposed TV method a great candidate for both types of MIT imaging.

Index Terms-Total variation regularization, Split Bregman, magnetic induction tomography, MIT inverse problem, eddy current forward problem

I. Introduction

Magnetic induction tomography (MIT) is an emerging new tomographic imaging technique, based on the measurement of mutual inductances in a coil array, which can be modeled by eddy current theories. MIT is able to produce reconstructed images of all three passive electromagnetic properties (PEP), i.e., permeability, permittivity and conductivity [1][2]. Initially, metallic based MIT was developed for molten metal flow monitoring [1]. In the past few years, low conductivity MIT has been primarily developed for medical imaging applications such as imaging brain function or stroke detection [3], and has lately being proposed as potential multi-phase flow imaging technique. High conductivity MIT has also been widely used in industrial applications such as non-destructive testing (NDT) for material characterization [4].

Although MIT is capable of imaging all PEP, it usually aims at visualizing the conductivity distribution of the object under test, which can be achieved by modeling eddy currents in the forward model [5] and then identifying the conductivity distribution inverse problem. The inverse problem in MIT is severely ill posed, so regularization is needed. Tikhonov regularization method, based on solving the least square solution, is widely used to solve the inverse MIT problem [6]. However, this leads to suboptimal results, with over smoothed reconstructed images that show blurred edges and boundaries between materials. A better option is to use an $l_1 - norm$ regularization, such as total variation (TV) functional, which has been shown to improve image quality in MIT and other applications, and has received considerable attention in the past few years [7][8][9]. However, the TV functional has few drawbacks. TV is non-differentiable, which is commonly avoided by using an approximation. Smooth approximations of TV can have an effect in image quality, blurring sharp edge [10]. This effect can be reduced by tuning the parameter that controls the approximation of TV, which can lead to slow down in convergence. In addition, TV method suffers from low contrast recovery [10][11].

Iterative methods based on the Bregman iteration have been proposed as a possible solution to these problems. The use of Bregman iterations for TV minimization introduced in [12] fixed the low contrast recovery problem of standard TV, by providing a sequence of solutions that allows to recover the contrast lost by the TV functional and to lead to lower error [10]. Furthermore, the split Bregman formulation presented in [13] further exploited Bregman iterations to provide an efficient method to minimize convex non-differentiable functional, like TV. This avoids the need of using smooth approximations of TV. In addition, the split Bregman method solves a constrained optimization problem, which has been shown to outperform the unconstrained TV problem and avoids choosing the regularization parameter with the L-curve or similar method [14][15]. However, the feasibility of split Bregman TV for improving image quality has not been assessed for MIT.

In this work, we compare Tikhonov and TV regularization methods and evaluate them on experimental MIT data. The TV problem is efficiently solved using the Split Bregman formulation. Methods are quantitatively evaluated on experimental phantoms in both low and high conductivity MIT settings.

II. Methodology

A. Forward problem

[1] Engineering Tomography Laboratory (ETL), Department of Electronic and Electrical Engineering, University of Bath, Bath, UK: Email: m.soleimani@bath.ac.uk
[2] Departamento de Bioingeniería e Ingeniería Aeroespacial, Universidad Carlos III de Madrid, España. Email: juanabascal78@googlemail.com
[3] Instituto de Investigación Sanitaría Gregorio Marañón (IiSGM) Madrid, Spain
[4] Centro de Investigación en Red de Salud Mental (CIBERSAM), Madrid, Spain

To solve the forward problem, the MIT domain is separated into two regions: the non-conductive region Ω_s and the eddy current region Ω_e, (Figure 1), where $\Omega_c = \Omega_s + \Omega_e$.

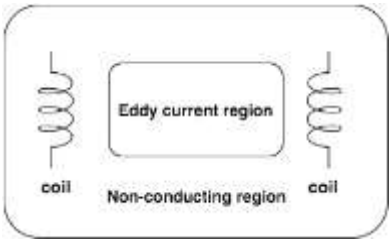

Figure 1: Domains in MIT forward model

The forward problem is solved using an edge finite element method (FEM), with the aid of magnetic vector potential (A) [16]. The (A, A) formulation, can be obtained from the Maxwell's equations [17]:

$$\nabla \times \frac{1}{\mu} \nabla \times A + j\omega\sigma A = J_s \tag{1}$$

where J_s is the source current density, σ is electrical conductivity and μ is magnetic permeability, and ω is angular frequency. Source current is modeled by Biot-Savart theory [18]

$$B_s = \int \frac{\mu_0 I}{4\pi|r|^3} \overrightarrow{dl} \times \vec{r} \tag{2}$$

where r is the distance between the current segment dl and the fixed point, and μ_0 represents the free space permeability. By introducing electric vector potential T_s, defined as,

$$J_s = \nabla \times T_s \tag{3}$$

In free space, according to the Ampere's law, the current density

$$J_s = \nabla \times H_s \tag{4}$$

so T_s can be described by H_s , and

$$H_s = \frac{1}{\mu_0} B_s \tag{5}$$

the equation (1) is transferred to

$$\nabla \times \frac{1}{\mu} (\nabla \times A) + jw\sigma A = \nabla \times T_s \tag{6}$$

We discretize equation (6) by applying Galerkin's formulation and introducing basis function N_i for edge FEM, which leads to the Galerkin's approximation [17,19].

$$\int_{\Omega_c} \left(\nabla \times N_i \cdot \frac{1}{\mu} \nabla \times A\right) dv + \int_{\Omega_c} (j\omega\sigma N_i \cdot A) dv = \int_{\Omega_s} (\nabla \times N_i \cdot T_s) dv \tag{7}$$

where N_i is the linear combination of edge shape functions and the right hand side in equation (7) can easily been calculated from equation (3), and Ω_C is entire region and Ω_S is the current source region (excitation coil). Then the induced voltage in measuring coil can be calculated by using the volume integration equation

$$V_{mn} = -j\omega \int_{\Omega_s} (A \cdot J_0)\, dv \tag{8}$$

where J_0 is the unit current density passing through coil. Due to the relationship between induced voltage in the sensing coil and conductivity, the element of the Jacobian matrix can be expressed by

$$\frac{\partial V_{mn}}{\partial \sigma_x} = -\omega^2 \frac{\int_{\Omega_x} A_m \cdot A_n dv}{I} \tag{9}$$

where A_m is the forward solver of excitation coil m excited by I, A_n is the forward solver of sensor coil excited by unit current, σ_x is the conductivity of pixel x and Ω_x is the volume of the perturbation.

B. Inverse problem

The inverse problem is defined as the retrieval of the unknown conductivity σ from the measured boundary voltage $V_{measured}$, represented by the nonlinear equation

$$V_{measured} = F(\sigma) + e \tag{10}$$

where F is the forward operator and e is the noise in the measurements. In MIT, it is common to linearize this equation for difference data [15]

$$V_{measured} - F(\sigma_0) = J(\sigma - \sigma_0) \tag{11}$$

where J is the Jacobian or sensitivity matrix ($J \in R^{m \times n}$), which can be obtained from forward problem. Let $\Delta\sigma = \sigma - \sigma_0$, $\Delta v = V_{measured} - F(\sigma_0)$ and σ_0 be the initial estimate conductivity, then equation (9) can be reduced to

$$\Delta v = J\Delta\sigma \tag{12}$$

The conventional method is to solve the least-square problem:

$$x_\alpha = argmin_{\Delta\sigma} \frac{1}{2} \|J\Delta\sigma - \Delta v\|^2 \tag{13}$$

- **<u>Tikhonov regularization method</u>**

Since the inverse problem is ill posed, a Tikhonov regularization penalty term $G_{TK}(\Delta\sigma)$ can be added to the optimization problem [20]

$$x_\alpha = argmin_{\Delta\sigma} (\|J\Delta\sigma - \Delta v\|^2 + G_{TK}(\Delta\sigma)) \tag{14}$$

$$G_{TK}(\Delta\sigma) = \gamma^2 \|R(\Delta\sigma - \Delta\sigma_0)\|^2 \tag{15}$$

where R is a regularization matrix and γ is the regularization parameter.

Minimizing this function means that the least square of the difference between measured voltage and the estimated voltage is minimized while the solution is kept reasonably close to the estimated image $\Delta\sigma_0$. The equation (14) to be minimized can be expanded as follows.

$$x_\alpha = argmin_{\Delta\sigma}\{M(\Delta\sigma)\} \quad (16)$$

$$M(\Delta\sigma) = \Delta\sigma^T J^T J\Delta\sigma - 2(\Delta v)^T J\Delta\sigma + \Delta v^T \Delta v + \gamma^2 [R\ (\Delta\sigma - \Delta\sigma_0)]^T [R\ (\Delta\sigma - \Delta\sigma_0)] \quad (17)$$

where equation (17) is the cost function. The minimum of cost function can be obtained by setting its first derivative equal to zero:

$$J^T\Delta v - J^T J\Delta\sigma - \gamma^2 R^T R\Delta\sigma + \gamma^2 R^T R\Delta\sigma_0 = 0 \quad (18)$$

After simplifying equation (18), it can be obtained:

$$(J^T J + \gamma^2 R^T R)\Delta\sigma = J^T\Delta v + \gamma^2 R^T R\Delta\sigma_0 \quad (19)$$

The standard Tikhonov method is obtained by replacing R by I, the identity matrix, R=I, and assuming $\Delta\sigma_0 = 0$,

$$\Delta\sigma = (J^T J + \gamma^2 I)^{-1} J^T\Delta v \quad (20)$$

Although standard Tikhonov is widely used for many applications, recently a hybrid Tikhonov regularization was shown to produce better imaging results [21]. To provide a fair comparison with the proposed TV algorithm we chose the most advanced hybrid Tikhonov method based on combining Laplacian and Tikhonov based regularization terms [21]

$$\Delta\sigma = (J^T J + \gamma^2 R_1 + \lambda^2 R_2)^{-1} J^T\Delta v \quad (21)$$

where R_1 is an Laplacian regularization term, R_2 is an identity matrix, and γ and λ are the regularization factors for R_1 and R_2, respectively. The hybrid Tikhonov method has good quality in challenging low conductivity MIT data [21]. Here we empirically selected the regularization parameters for low conductivity and high conductivity reconstruction and used the same parameters in all experimental studies.

- **Total variation problem solved using the Split Bregman formulation**

The total variation problem is defined by adding a penalty term to equation (15), the $l_1 - norm$ of the gradient of the image, or the so called, total variation regularization term $G_{TV}\ (\Delta\sigma)$

$$G_{TV}\ (\Delta\sigma) = \alpha R(\Delta\sigma) = \alpha\|\nabla\ \Delta\sigma\|_1 \quad (22)$$

where α is the regularization parameter, ∇ is the gradient and $\|\cdot\|_1$ is the $l_1 - norm$. We used an isotropic version of the TV functional as proposed in [13] given by

$$\|\nabla\ \Delta\sigma\|_1 = \sum_i \sqrt{(\nabla_x\Delta\sigma)_i^2 + \left(\nabla_y\Delta\sigma\right)_i^2} \quad (23)$$

Then the problem we wish to solve is the constrained optimization problem

$$x_\alpha = argmin_{\Delta\sigma}\alpha\|\nabla\Delta\sigma\|_1 \quad such\ that\ \ \|J\Delta\sigma - \Delta v\|^2 < \rho \quad (24)$$

which can be solved using standard constrained optimization algorithms. However, these methods are computationally demanding for large-scale problems. In addition, the TV functional is not differentiable, which is usually avoided by substituting TV by an approximated functional.

TV regularization was applied to metallic MIT in [8][9], so further evaluation was needed for low conductivity MIT. Additionally, a more efficient approach is to use the Bregman iteration, which is an iterative method based on Bregman distance [12]. For a given convex function $C\ (x)$, the Bregman distance between x and y can be defined as

$$D_C\ (x, y) = C\ (x) - C\ (y) - < s, x - y > \quad (25)$$

where s is the subgradient of C at y, and $<,>$ denotes the scalar product. In this case, we set $C\ (x) = \alpha R\ (x)$ be the total variation function and assume that $\Delta\sigma$ is the optimal solution and $\Delta\sigma^k$ is the iterative solution. Then, the Bregman iterative algorithm equivalent to equation (24) can be expressed as

$$\Delta\sigma^{k+1} = argmin_{\Delta\sigma}\ D_{\alpha R}\ (\Delta\sigma, \Delta\sigma^k) + \frac{\lambda}{2}\|J\Delta\sigma - \Delta v\|^2 \quad (26)$$

where the subgradient of the total variation function at the $(k+1)\ th$-iteration is

$$s^{k+1} = s^k - \lambda J^T(J\Delta\sigma^{k+1} - \Delta v) \quad (27)$$

Equation (26) and (27) are the basic formulation of Bregman iterative algorithm, which can be simplified to [15]

$$\Delta\sigma^{k+1} = argmin_{\Delta\sigma}\{\alpha R\ (\Delta\sigma) + \frac{\lambda}{2}\|J\Delta\sigma - (\Delta v)^k\|^2\} \quad (28)$$

$$(\Delta v)^{k+1} = (\Delta v)^k + \Delta v - J\Delta\sigma^{k+1} \quad (29)$$

Based on the Bregman iterative algorithm, split Bregman methods can extend the utility of the Bregman iteration to the minimizations of more general $l_1 - norm$ regularization terms.

Equation (28) can be solved now at each iteration with conventional unconstrained optimization algorithms. However, the term $R\ (\Delta\sigma)$ is non-differentiable and difficult to minimize. The Split Bregman iteration method is introduced to address this. An auxiliary variable d can be used to convert equation (28) to a constrained optimization problem, easier to solve

$$(\Delta\sigma, d) = argmin_{\Delta\sigma,d}\frac{1}{2}\|J\Delta\sigma - \Delta v^k\|^2 + \alpha\|d\|_1 \quad such\ that\ \ d = \nabla\ \Delta\sigma \quad (30)$$

To solve this constrained problem, we as above, after applying the Bregman iteration method, the equation (30) can be written as

$$(\Delta\sigma^{k+1}, d^{k+1}) = argmin_{\Delta\sigma,d}\frac{1}{2}\|J\Delta\sigma - \Delta v^k\|^2 + \alpha\|d\|_1 + \frac{\beta}{2}\left\|d - \nabla\Delta\sigma - b_d^k\right\|^2 \quad (31)$$

$$b_d^{k+1} = b_d^k + \nabla\Delta\sigma^{k+1} - d^{k+1} \quad (32)$$

Then minimizing equation (31) can be achieved by minimizing $\Delta\sigma$ and d separately as following [13, 14]:

- $\Delta\sigma^{k+1} = argmin_{\Delta\sigma} \frac{1}{2}\|J\Delta\sigma - \Delta v^k\|^2 + \frac{\beta}{2}\left\|d^k - \nabla\Delta\sigma - b_d^k\right\|^2$
- $d^{k+1} = argmin_d \alpha\|d\|_1 + \frac{\beta}{2}\left\|d - \nabla\Delta\sigma^{k+1} - b_d^k\right\|^2$

Solutions to $\Delta\sigma^{k+1}$ and d^{k+1} are given by analytic expressions that can be efficiently computed [13]. Hence, the split Bregman method provides a sequence of solutions $(\Delta\sigma^{k+1}, d^{k+1})$ that converges to the solution of the constrained optimization problem (24). One of the benefits of the split Bregman formulation is that it does not require explicit calculation of the derivatives of the TV functional, which must be otherwise approximated because of the no differentiability of the TV functional. These approximations used by more standard approaches are generally non optimal and lead to slow convergence.

C. Experimental setup

Experimental data were acquired from two different MIT systems. MIT system comprises the measuring subsystem, conditioning electronics part, data acquisition & processing subsystem, and the computer used to reconstruct and process the images. Though there are some different types of MIT systems, the characteristics of their components are nearly the same to some degree. The measuring subsystem includes an array of coils placed around the measuring space. The size, number and position of the coils vary in different MIT systems. The conditioning electronics consist of amplification circuit, precision rectifier and low pass filtering. During the experimental process, two sets of measurement are acquired, background data (B) and the measuring data ($B + \Delta B$). Background data, considered as reference data, are obtained without any object in the measuring space, while measuring data are captured with the target in the measuring space. After recording these two datasets, the difference between them produces the information of the perturbation signal (ΔB). In this experimental study, two types of MIT system have been used.

- **Low conductivity MIT system**

The MIT system described in this section is the Bath MK-III system (see Figure 2), designed for low conductivity sample imaging. It consists of the following components,

- A signal generator
- A National Instrument based data acquisition system (NI PXIe-1073)
- A sensor array containing 16 air-core inductive and metallic shields, the diameter of the tank is 23cm.
- A host computer

Figure 2: Bath MK-III magnetic induction tomography system

The working frequency of this system is selected to be 13MHz and the LabView program is used to control the signal generator and to achieve the data acquisition/ channel switching tasks [22]. The channel-switching card NI2593 was employed in our system to accomplish the 2×8: 1 multiplexer scheme, and thus 8 coils were dedicated to transmitters while the other 8 coils were dedicated to receivers. So the data collection pattern of this system is as following: Tx1-Rx2, Tx1-Rx3, …Tx1-Rx7, Tx2-Rx3, Tx2-Rx4, …Tx2-Rx8, …and Tx8-Rx6, which can provide $8 \times (8 - 2) = 48$ measurements. Then the image reconstruction system extracts those independent measurements to LabView and Matlab program to display the reconstructed images.

- **High conductivity MIT system**

The Bath MK-II system (Figure 3) consists of the following components:

- A signal generator
- A National Instrument based data acquisition system (NI USB-6259)
- A channel switching board
- A sensor array containing several inductive coils
- A host computer

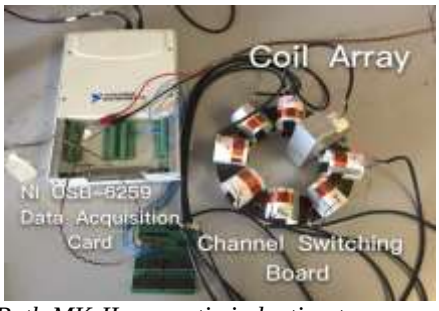

Figure 3: Bath MK-II magnetic induction tomography systems

The channel switching process can be accomplished by the ADG406 multiplexers, which is a 16:1, monolithic CMOS analogue multiplexer, and thus when the first coil is set as the transmitting coil, the rest of the coils are reading the measurements sequentially. For a MIT system with a n number of coils, the unique coil pairs are 1-2,1-3,1- n…2-3,2-$(n-1)$…$(n-1)$- n. The data collection pattern can be described as the following sequence: exciting coil 1 as the first cycle and measuring voltage from the other coils (2 to $n-1$); exciting coil 2 as the second cycle, and measuring the voltage from coil 3 to coil $n-1$, and so on and so forth. This provides $m = n\,(n-1)/2$ independent measurements, which are imported

into the image reconstruction. In the case of 8-channel system, there are $\frac{8\times7}{2} = 28$ measurements.

D. Data sets

Seven experimental datasets were acquired with low conductivity and high conductivity MIT systems. Four sets of experimental tests were carried out for low conductivity MIT system in Figure 2 at a frequency of $13MHz$. The other three sets of experimental tests were carried out for high conductivity MIT system in Figure 3 by setting amplitude to $15V_{p-p}$ and frequency to $100kHz$. Free space measurements data were selected to be the background data.

All datasets were reconstructed using both Tikhonov and total variation regularization methods.

III. Results

A large number of experimental data was used to evaluate these two algorithms. These experiments are numbered from L1-L28, which will be used in image analysis in section (V).

A. Low conductivity MIT

- Test 1 in low conductivity MIT

The experimental setup can be seen in Figure 4. The conductivity of background is 1.58 S/m and the samples tested were four insulating inclusion bottles, with diameters of 2, 6.5, 9.5 and 13 cm.

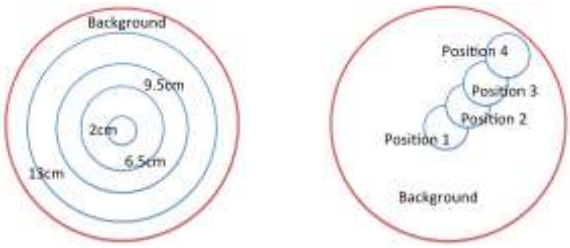

(a) Four different sizes of inclusion *(b) Displacement of inclusion*

Figure 4: The real experimental setup.

Table1 and Table2 show the images reconstructed by Tikhonov regularization and Total variation regularization algorithms. Reconstructed images are shown for bottles with 2, 6.5, 9.5 and 13 cm diameter (in row) and for different positions of the bottle (in column).

Table 1. Reconstructed images of different sizes samples in position 1 and position 2

Diameter	Algorithm	Position 1 (L1-L4)	Position 2(L5-L8)
2 cm	Tikh.	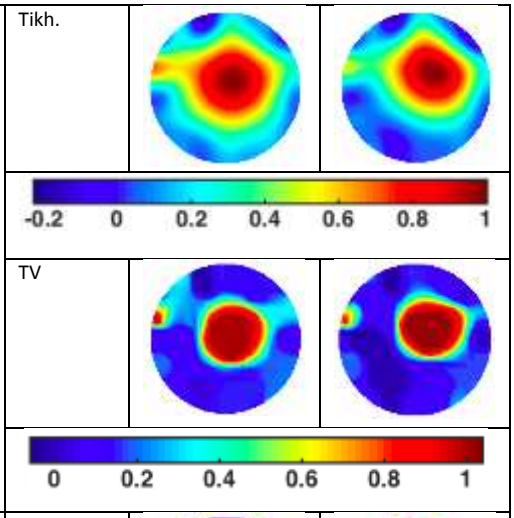	
	TV		
6.5 cm	Tikh.		
	TV		
9.5 cm	Tikh.		
	TV		
13 cm	Tikh.		

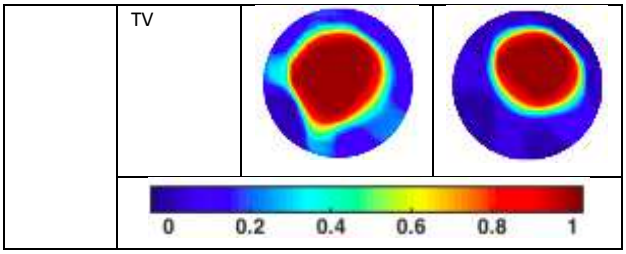

Table 2. Reconstructed images of different sizes samples in position 3 and position 4

Diameter	Algorithm	Position 3(L9-L12)	Position 4(L13-L16)
2 cm	Tikh.	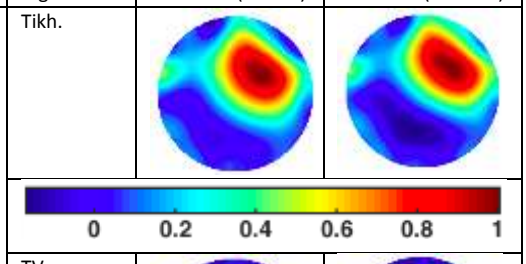	
	TV	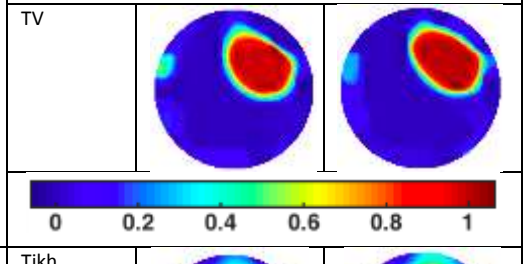	
6.5 cm	Tikh.	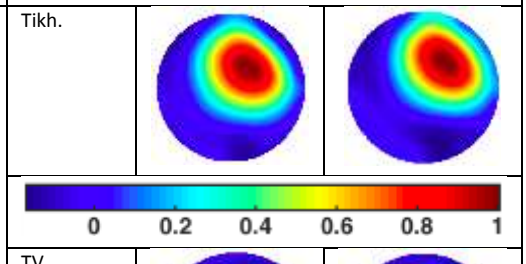	
	TV	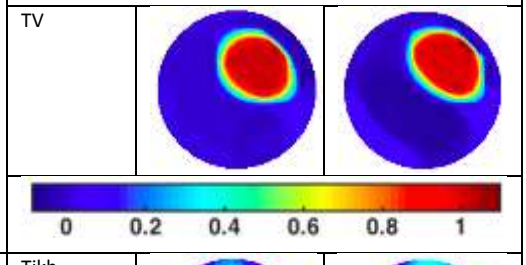	
9.5 cm	Tikh.	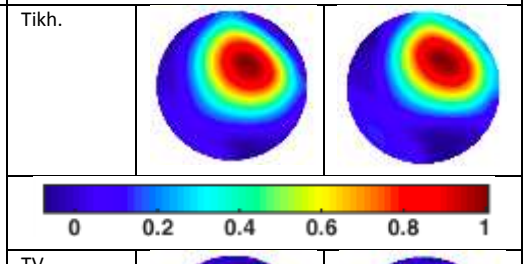	
	TV	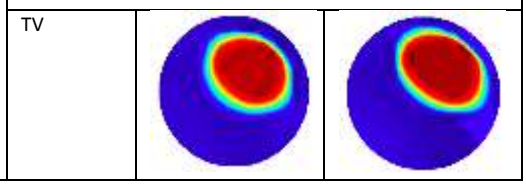	

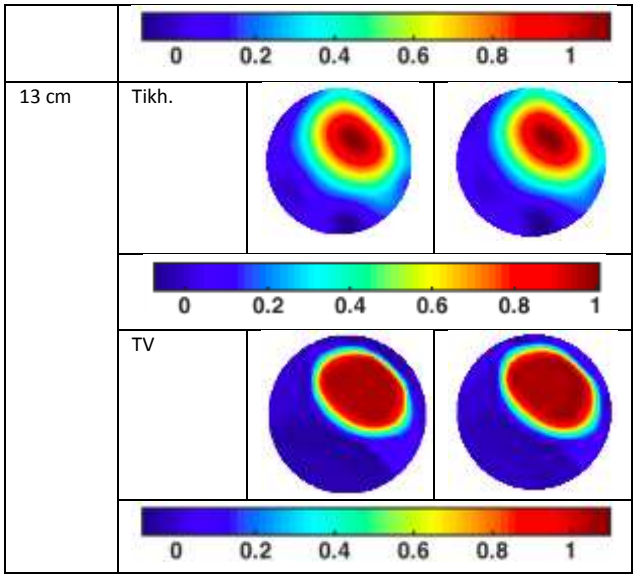

- Test 2 in low conductivity MIT

The experimental setup can be seen in Figure 5. The samples tested were two bottles of 0.9% saline water in two different positions, while the background was free space or tap water. The conductivity of 0.9% saline water samples is 1.58 $^{S}/_{m}$ and the conductivity of this tap water background is 0.06 $^{S}/_{m}$.

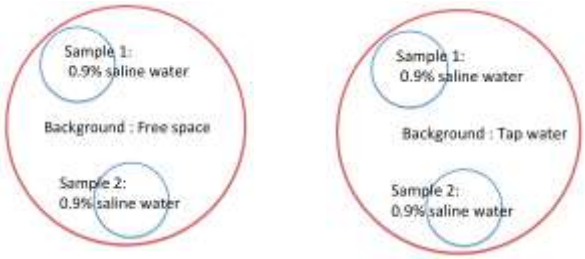

(a) Background-free space (b) Background- tap water

Figure 5: The real experimental setup.

Table 3 and 4 show separately the reconstructed images obtained when the background is free space and tap water. The images show reconstructions by Tikhonov regularization and Total variation regularization method for first inclusion, second inclusion and both inclusions together.

Table 3. Reconstructed images of two bottles saline water in free space background

	Sample1 (L17)	Sample2 (L18)	Sample 1+2 (L19)
Tikh.	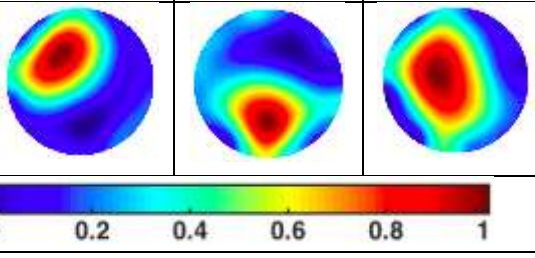		

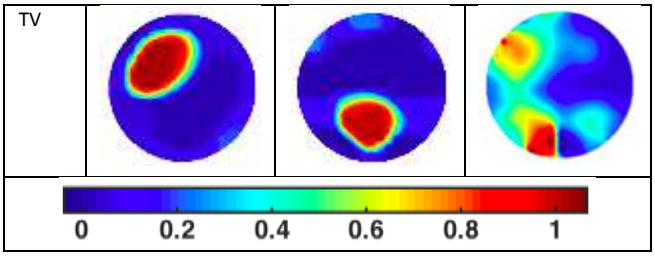

Table 4. Reconstructed images of two bottles saline water in tap water background

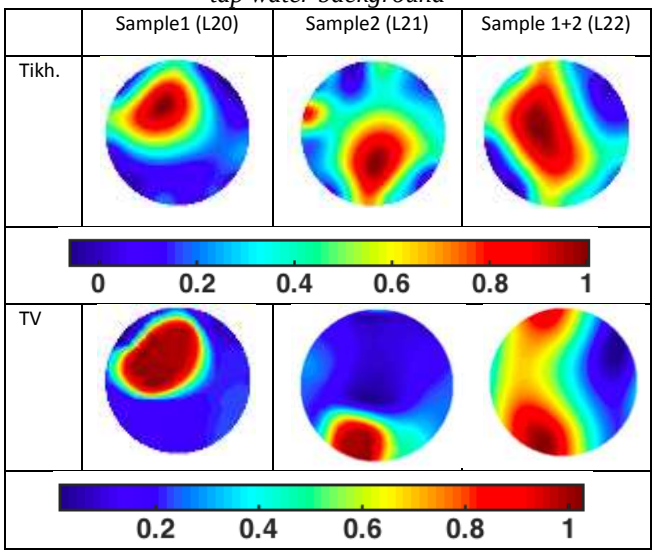

- Test 3 in low conductivity MIT

The experimental setup can be seen in Figure 6. The background was 3% saline water and the samples were three bottles of different sizes with inclusion of 0.9% saline water.

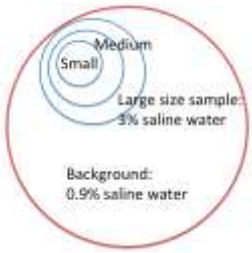

Figure 6: Experimental setup in Test 3.

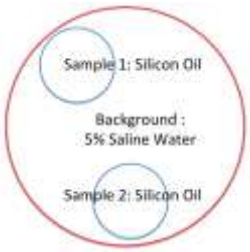

Figure 7: Experimental setup in Test 4.

Table 5 shows the reconstruction images for Tikhonov regularization and Total variation regularization method for small, medium and large size of inclusion.

Table 5. Reconstructed images of three different sizes samples in 0.9% saline water background

	Small size (L23)	Medium size (L24)	Large size (L25)

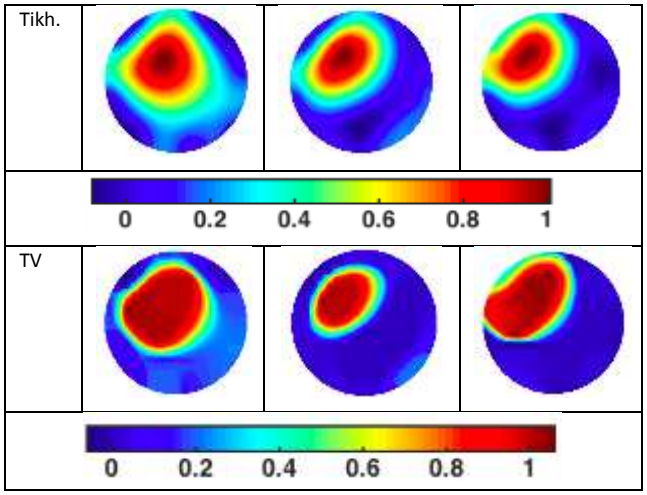

- Test 4 in low conductivity MIT

The experimental setup can be seen in Figure 7. The samples tested were two bottles of silicon oil working as non-conductive inclusions and 5% saline water considered as conductive background.

Table 6 shows the reconstruction images obtained by Tikhonov regularization and Total variation regularization methods, where columns correspond to one silicon oil inclusions, silicon oil inclusion at a different position and two silicon oils inclusions together.

Table 6.Reconstructed images of two bottles of silicon oil in 5% saline water background

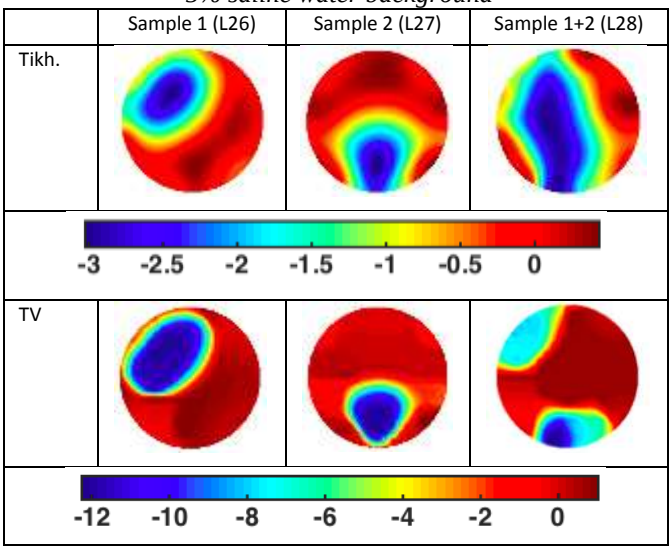

B. High conductivity MIT

High conductivity MIT experiments involves 9 experiments (we call them H1-H9), which includes various positioning of metallic sample (s).

- Test 5 in high conductivity MIT

The sample tested in Test 5 was a rectangular aluminum object, and the experimental setup is shown in Figure 8.

(a) Real conductive distribution in position 1

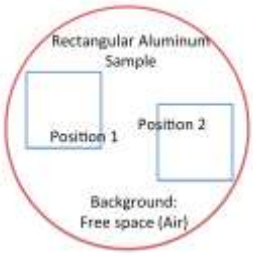

(b) Rectangular aluminium sample in position 1 or 2

Figure 8. Experimental setup.

Table 7 shows the images reconstructed using Tikhonov and Total variation regularization methods for two positions of the steel sample.

Table 7. Reconstructed images of a rectangular aluminum sample in position 1 and position 2

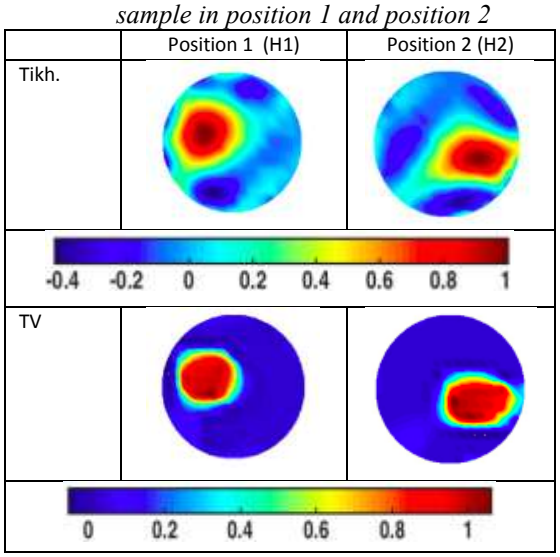

- Test 6 in high conductivity MIT

Test 6 is a circular aluminum sample placed in four different positions and the experimental setup is shown in Figure 9.

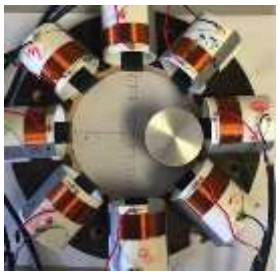

(a) Real conductive distribution in position 1

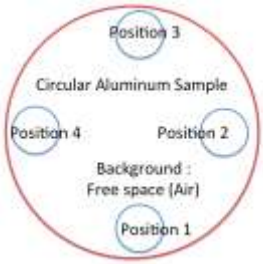

(b) Circular aluminum sample in position 1,2,3,4

Figure 9. Experimental setup.

Table 8 shows the reconstruction images obtained by this test. The images correspond to reconstructions by Tikhonov and Total variation regularization algorithm for four different positions of the sample.

Table 8. The images of a circular aluminum sample in four different positions

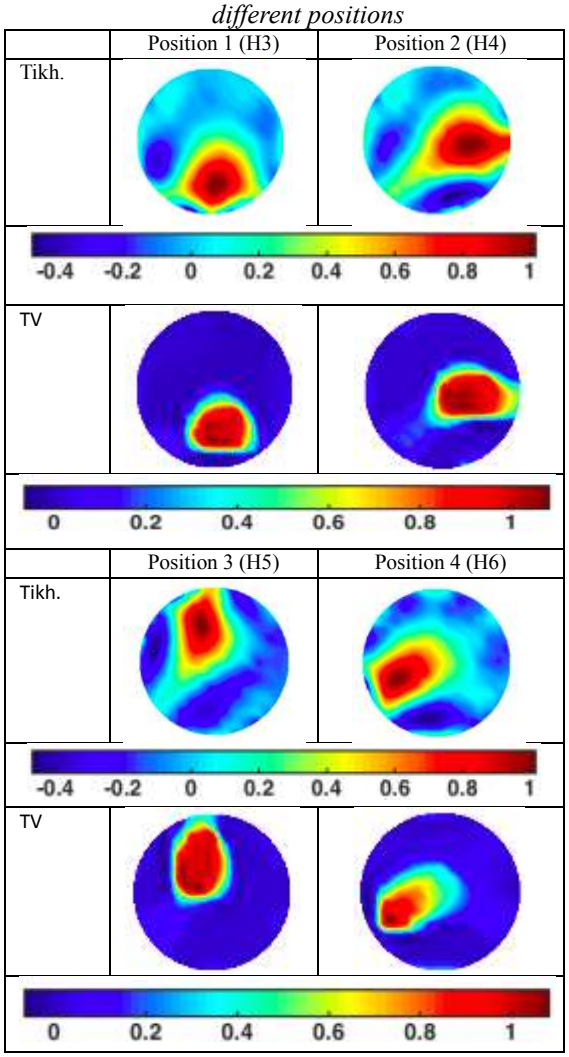

- Test 7 in high conductivity MIT

Test 7 used two circular aluminum samples placed in different positions separately (shown in Figure10).

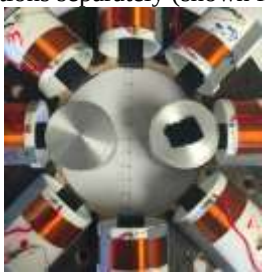

(a) Real conductive distribution

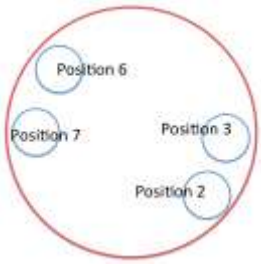

(b) Two samples in different positions separately

Figure 10. Experimental setup.

Table 9 shows the reconstructed images obtained after this test by Tikhonov and Total variation regularization algorithms, for two circular aluminum samples in different positions separately.

Table 9. Reconstructed images of two circular aluminum samples in different positions

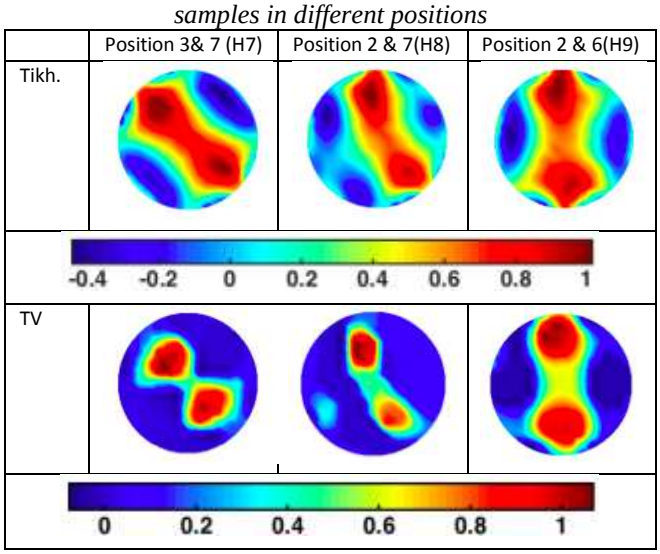

IV. Result analysis and discussions

It can be seen from imaging results of both low conductivity and high conductivity samples that TV can produce higher quality images. To further demonstrate this, the image quality measures are used to quantitatively show comparison between TV and Tikhonov based algorithms. In this case shape deformation (SD), resolution (RES) and amplitude ration (AR) was selected from GREIT image quality parameters [23]. SD shows part of reconstructed images (after some theresholding) that does not fit in a circular shape. For higher quality reconstruction SD should be low and uniform for the same sample size and shape. Resolution (RES) measures the size of reconstructed inclusion as a fraction of size of entire imaging region; this is equivalent to a measure of point spread function (PSF) size. RES should be uniform and small, in order to more accurately represent shape of the inclusion based on their conductivity values. AR measures the ratio of image pixel amplitudes in the inclusion area to that in the reconstructed image. A uniform and smaller AR is a measure of higher quality image. GREIT parameters are widely used for image quantification and quality measures, we refer to [23] for more detailed descriptions. Figure 11 show SD, RES, and AR, for low conductivity experiments from L1-L28. Apart from very few points in SD, the TV are universally outperforms the Tikhonov algorithm in terms of all image quality measures. The fact that the neighboring measurements were excluded in low conductivity MIT system, this sometimes create some deformation in shape of inclusions as this act as missing data MIT, this is perhaps responsible for larger numbers for SD, and size dependent SD in both algorithms.

Figure. 12 show SD, RES and AR for 8 experiments in high conductivity objects. Apart from SD for experiment H9, in all other examples the TV shows better performance compared to standard Tikhonov method.

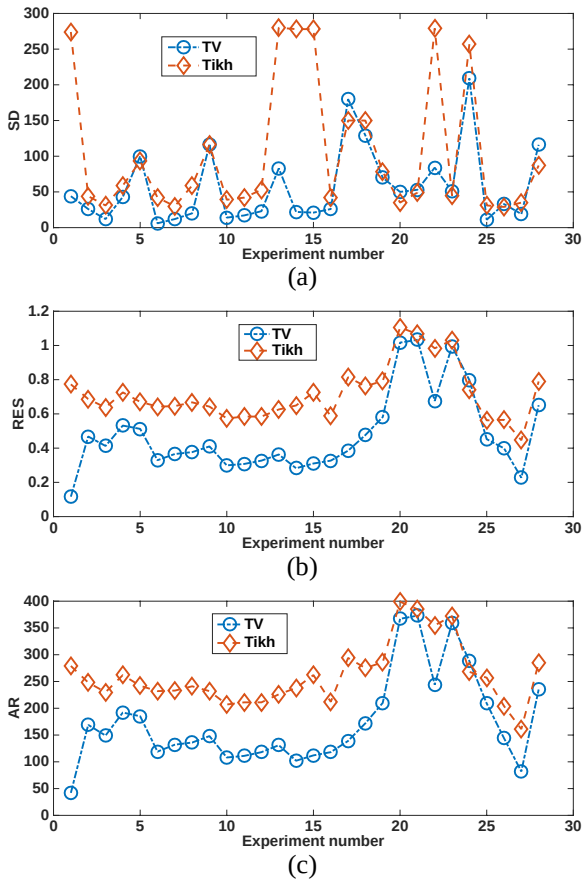

Figure 11. Figures of merit for experiments L1-L28 in metallic sample(s)

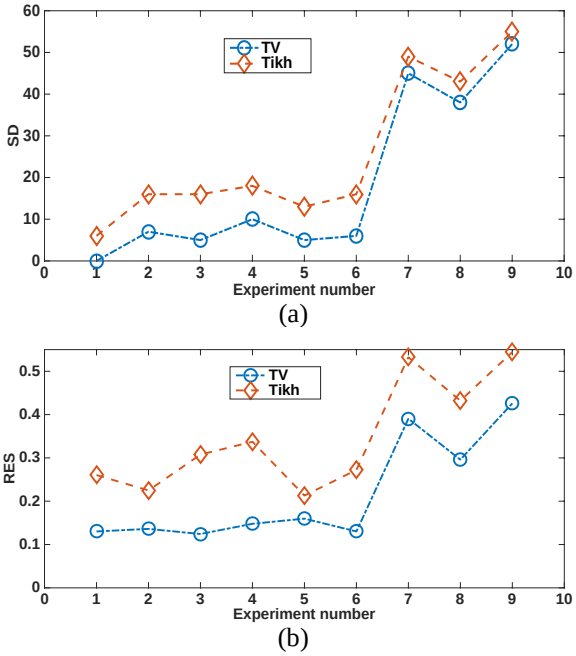

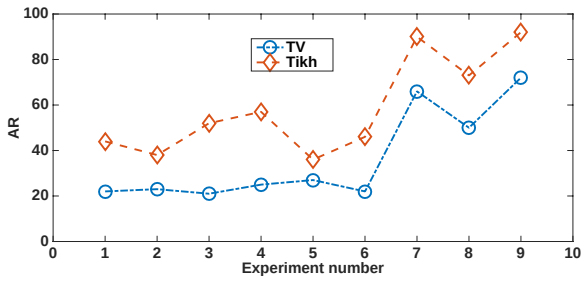

(c)

Figure 12. Figures of merit for experiments H1-H9 in metallic sample(s)

The total variation method produced reconstructed images with improved quality for both low conductivity and high conductivity MIT systems. As it can be seen from the results, the differences in the dimension and position of the objects cannot be distinguished from the reconstructed images obtained by Tikhonov regularization method but total variation lead to improved recovery of the size and shape of the target and in particular sharper boundaries between different conductivity regions.

Previous work for MIT has used Tikhonov method for conductivity flow imaging [21], which evaluated several saline solutions with different dimensions/conductivity values in a low conductivity MIT system. The results presented in [21] showed that the reconstructed images are smooth enough but in the case of testing two or more objects simultaneously, the reconstruction could not reliably recover conductivity contrasts and imaging resolution. However, according to our experimental results, total variation method improved conductivity contrast in all these images. Moreover, in this work, we have proposed and validate the use of the split Bregman method for minimizing the TV problem in MIT and have compared it to commonly used Tikhonov method. Previous studies have shown that Bregman iteration methods for TV correct some of the deficiencies of standard TV and lead to improve results [10][13][14]. A comparison between different types of TV and Bregman-based TV methods in MIT will be considered in further work. This paper comprehensively demonstrate the advantage of TV method against commonly used method.

It is common practice in MIT to use linear for experimental difference data, which is more robust and less sensitive to the effect of modeling error and noise in measured data. The proposed been validated using experimental data covering a wide range of scenarios, with different size and location of inclusions. However, the validation has focused on 2D, so further studies need to be done to address the 3D inverse problem. Besides, due to the nature of eddy currents, the MIT forward problem is a large-scale problem, which will increase the demand of computational resources. Extension to nonlinear with experimental data and absolute imaging is still remaining a challenging, partly due to lack of good experimental data and matching with the forward models.

Overall, image quality parameters show consistency good performances in both low and high conductivity case, but as expected metallic MIT tests shows more robust imaging results. Some experiments in low conductivity case present more challenges dues to low conductivity contrasts between background and inclusions. In these cases TV performed well enough to recover images that not recovered well by Tikhonov algorithm.

V. Conclusion

A TV method based on the Split Bregman formulation, is presented and validated experimental MIT data. Quantitative image quality analysis shows significant improvement of image qualities by using proposed TV algorithm. In experimental work presented here the total variation algorithm produced high quality images, making it a suitable candidate for image reconstruction in both metallic imaging and low conductivity MIT imaging. It is anticipated that the high quality images that can be obtained using TV algorithm and its robustness against image reconstruction parameters, can help stimulate new applications for MIT in both industrial tomography and medical imaging.

Reference

1. Wei, H.Y. and Soleimani, M., 2012. A Magnetic Induction Tomography System for Prospective Industrial Processing Applications. Chinese Journal of Chemical Engineering, vol. 20(2), pp. 406-410
2. Ma, X., Peyton, A.J., Binns, R., Higson, S.R., Electromagnetic techniques for imaging the cross section distribution of molten steel flow in the continuous casting nozzle. IEEE Sensors Journal 5 (2005) 224–232.
3. Gwan Soo, P. and Dong Seok, K., 2005. Development of a magnetic inductance tomography system. IEEE Transactions on Magnetics, vol. 41(5), pp. 1932 – 1935.
4. Borges, AR., De Oliveira, JE., Velez, J., Tavares, C., Linhares, F. and Peyton, AJ. 1999. Development of electromagnetic tomography (EMT) for industrial applications. Part 2: Image reconstruction and software framework. *Proc. 1st World Congress on Industrial Process Tomography, Buxton, UK, 14–17 April*, pp. 219–25.
5. Caeiros, J. M. S. and Martins, R. C. 2012. An Optimized Forward Problem Solver for the Complete Characterization of the Electromagnetic Properties of Biological Tissues in Magnetic Induction Tomography. IEEE Transactions on Magnetics, vol. 48(12), pp.4707-4712.
6. Soleimani, M. 2008. Computational aspects of low frequency electrical and electromagnetic tomography: A review study. International Journal of Numerical Analysis and Modeling, vol. 5 (3), pp. 407-440.
7. Puwal, S. and Roth, B.J., 2011. Fourier analysis in magnetic induction tomography: mapping of anisotropic, inhomogeneous resistivity, Measurement Science and Technology, vol. 22(8). pp. 085802.
8. Soleimani M, Lionheart WRB, Peyton AJ, Ma X, and Higson S. R., " A three-dimensional inverse finite-element method applied to experimental eddy current imaging data," *IEEE Trans. Magn,*. vol.42, no. 5, pp. 1560-1567, May 2006

9. Yin W, Chen G , Chen L, Wang B, The Design of a Digital Magnetic Induction Tomography (MIT) System for Metallic Object Imaging Based on Half Cycle Demodulation, IEEE Sensor Journal, vol. 11, no. 10, pp. 2233-2240, 2011
10. Burger, M. and Osher, S. 2013. *Level Set and PDE Based Reconstruction Methods in Imaging: A guide to TV zoo.* Volume 2090 of the series Lecture Notes in Mathematics, pp.1-70.
11. Sawatzky, A., Brune, C., Kosters, T., Wubbeling, F. and Burger, M. 2013. *Level Set and PDE Based Reconstruction Methods in Imaging: EM-TV Methods for Inverse Problem with Poisson Noise.* Volume 2090 of the series Lecture Notes in Mathematics, pp.71-142.
12. Osher, S., Burger, M., Goldfarb, D., Xu, J.J. and Yin, W.T. 2005. An iterative regularization method for total variation based image restoration. Multiscale Modeling & Simulation, vol. 4(2), pp. 460-489.
13. Goldsteom, T. and Osher, S. 2009. The split Bregman method for L1-regularized problems. SIAM Journal on Imaging Sciences. vol. 2(2), pp. 323-343.
14. Abascal, J.F.P.J., Chamorro-Servent, J., Aguirre, J., Arridge, J., Correia, T., Ripoll, J., Vaquero, J.J. and Desco, M. 2011, Fluorescence diffuses optical tomography using the split Bregman method. Journal of Medical Physics, vol. 38 (11), pp. 6258.
15. Wang, J., Ma, J.W., Han, B. and Li, Q. 2012. Split Bregman iterative algorithm for sparse reconstruction of electrical impedance tomography. Signal Processing, vol. 92 (12), pp. 2952-2961.
16. Biro, O. and Preis, K. 2000. An edge finite element eddy current formulation using a reduced magnetic and a current vector potential. IEEE Transactions on Magnetics, vol. 36(5), pp. 3128–3130.
17. Biro, O. 1999. Edge element formulations of eddy current problems. Journal of Computer Methods in Applied Mechanics and Engineering, vol. 169(3), pp.392 pp. 391-405.
18. Tavares, RS., Martins, TC. and Tsuzuki, MSG. 2012. Electrical impedance tomography reconstruction through simulated annealing using a new outside-in heuristic and GPU parallelization. Journal of Physics: Conference Series, vol. 407(1), pp. 012015.
19. Biro, O. and Preis, K. 1989. On the use of the magnetic vector potential in the finite element analysis of three-dimensional eddy currents. IEEE Transaction on Magnetics, vol. 25 (4), pp. 3145-3159.
20. Merwa, R., Hollaus, K., Brunner, P. and Scharfetter, H. 2005. Solution of the inverse problem of magnetic induction tomography (MIT). Journal of Physiological Measurement, vol. 26(2), pp. S241–S250.
21. Ma, L., Hunt, A. and Soleimani, M. 2015. Experimental evaluation of conductive flow imaging using magnetic induction tomography. International Journal of Multiphase Flow, vol 72, pp. 198-209.
22. Wei, H.Y. and Wilkinson, A.J. 2011. Design of a sensor coil and measurement electronics for magnetic induction tomography. IEEE Transactions on Instrument and Measurement, vol. 60 (12), pp. 3853-3859.
23. Adler A et al 2009, GREIT: A unified approach to 2D linear EIT reconstruction of lung images Physiol. Meas. 30 S35-55.